The interstellar medium and star formation in nearby galaxies

Ludwig Biermann Award Lecture 2013

F. Bigiel⋆, **D. Cormier,** and **T. Schmidt**

Institut für theoretische Astrophysik, Zentrum für Astronomie der Universität Heidelberg, Albert-Ueberle Str. 2, 69120 Heidelberg, Germany

In this overview article we present some of the key projects we pursue in our Emmy Noether group. Our work is focused on nearby galaxies, where we use multi-wavelength, state-of-the-art survey data to probe distribution, abundance and properties of gas and dust in the interstellar medium (ISM) on ∼ kpc scales. We study the average, radial distributions of atomic (H I) and molecular hydrogen (H_2) across the disks of spiral galaxies and assess local (on 1 kpc scales) correlations between H I, H_2 and star formation rate (SFR) surface densities across the inner, optical disks of our sample of ∼ 30 spiral galaxies. The short H_2 depletion times (∼ 2 Gyr) we find raises the question of if and how star formation is refueled in galactic disks. We look for such signatures of radial gas flows in our H I data and find compelling evidence at least in one case. We extend and compare our gas-SFR studies to the outer disks of galaxies, where conditions change significantly in the ISM, e.g., low metallicity and dust abundance. We focus on star formation at low-metallicity further with detailed ISM studies in dwarf galaxies, where we combine spectroscopic observations in the infrared with detailed modelling to learn about composition and detailed physical properties of the ISM. Of particular interest is the question of what drives large scale star formation in galaxies at low metallicity.

1 Introduction

In this article we provide an overview over some of the key projects in our Emmy Noether group in Heidelberg. We focus on observational studies of the interstellar medium (ISM) and star formation (SF) in mostly nearby (distances of a few Mpc) galaxies.

Star formation is a key process in the context of galaxy evolution: It shapes the ISM of galaxies via feedback processes, determines the properties of stellar populations we observe at UV, optical and near-IR wavelengths and it regulates the physical properties and chemical enrichment of the ISM in galaxies. Thus, to understand how galaxies evolve, we must develop a thorough understanding of the star formation process and its interrelation with the ISM.

Galaxies in the Local Group and out to distances of a few Mpc cover a "sweetspot" for these kind of studies: compared to the Milky Way there is no distance ambiguity, they offer a wide range of galactic environments and physical conditions to probe (e.g. metallicity), and the outside perspective allows to distinguish different regimes within individual galaxies (arm-interarm, center-outskirts, etc.). Compared to more distant galaxies, nearby galaxies offer much better resolution, sensitivity and wavelength coverage: the same galaxies have been targeted with virtually every telescope from the X-ray to the radio. These circumstances

⋆ Corresponding author: bigiel@uni-heidelberg.de

makes them ideal targets to study the detailed properties of the ISM and how these are related to the star formation process in galaxies.

In particular the last decade has seen an explosion in such multi-wavelength data sets ideally suited to probe the ISM and SF in nearby galaxies. This includes optical, UV (GALEX) and IR (*Spitzer*, *Herschel*) data, all of which have resolutions as good as a few arcseconds. To complete a detailed picture of the ISM, however, missing ingredients for many years were deep, extended and systematic observations of the distributions of the atomic (H I) and molecular (H_2) gas in a matched set of nearby galaxies.

This situation was remedied by two large surveys our team is involved in: "The H I Nearby Galaxy Survey" (THINGS, Walter et al. 2008) and the "HERA CO-Line Extragalactic Survey" (HERACLES, Leroy et al. 2009). THINGS is a large program carried out at the NRAO VLA and provides the distribution of the warm, neutral, atomic hydrogen by mapping the H I 21 cm emission at a resolution of ∼ 10″ for 34 nearby spiral and dwarf irregular galaxies. Many disk galaxies have extended, massive H I distributions (compare Fig. 10), which provide the ultimate fuel for star formation in galaxies. More intimately related to ongoing star formation in galaxies is the distribution of the colder (< 100 K), denser ($\sim 10^2$–10^3 cm^{-3}) molecular hydrogen (H_2), which cannot be observed directly, however. The H_2 molecule lacks a dipole moment and temper-
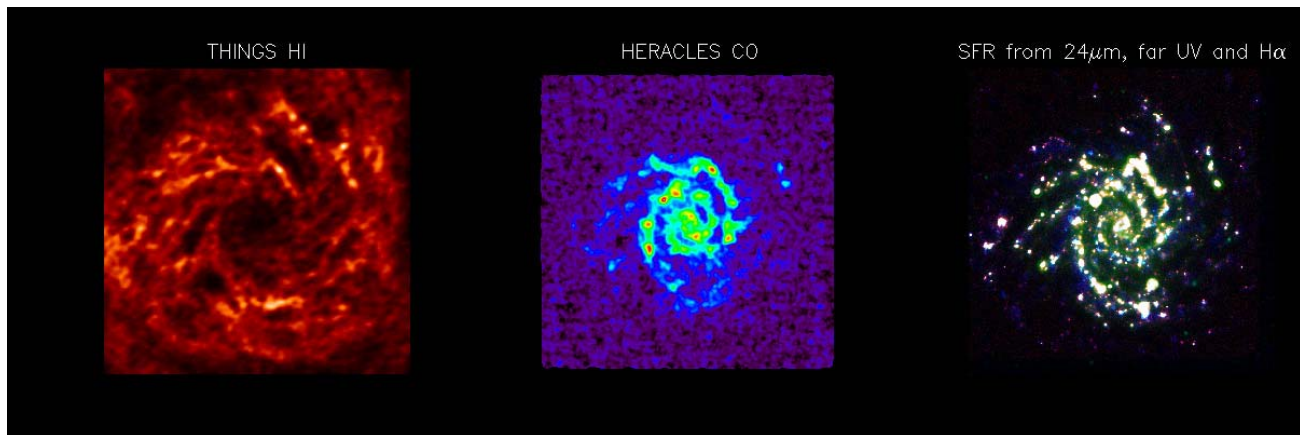
Fig. 1 The multi-wavelength data set available for the 30 nearby disk galaxies shown in Table 1, illustrated for NGC 6946.

atures in molecular clouds are too low to excite quadrupole or vibrational transitions. Therefore emission from the CO molecule is commonly used as a tracer, where inferring H_2 masses or surface densities depends on careful calibration of a conversion factor (for which we assume a constant Milky Way value of $2 \times 10^{20}\,\mathrm{cm^{-2}\,(K\,km\,s^{-1})^{-1}}$, see review in Bolatto et al. (2013). In order to obtain information on distribution and abundance of the molecular gas, we used the IRAM 30 m telescope to map the distribution of CO emission across the same sample of galaxies as part of the HER-ACLES survey. Mapping large areas was made possible due to the availability of the, at the time, new HERA receiver array (Schuster et al. 2007), allowing for efficient and deep wide-field mapping in the 1 mm atmospheric window.

With these two data sets, a comprehensive multi-wavelength data base for a matched set of nearby galaxies (listed in Table 1) was put in place, ranging from the UV, over optical broad and narrow band (e.g. Hα emission) to the IR (*Spitzer*, *Herschel*) as well as mm (IRAM) and cm (NRAO VLA) wavelengths (Fig. 1). The highest resolution achievable for the data set is limited by the radio data and is about $15''$. This corresponds to physical scales of around a kpc at the median distance of the galaxy sample shown below.

This overview article is organized as follows: In Sect. 2 we discuss the average radial distributions of atomic and molecular gas in these galaxies; in Sect. 3 we present a search for radial gas flows in the H I velocity fields; in Sect. 4 we focus on relations between star formation and H I and H_2 distribution and abundance, and in Sect. 5 we show results regarding the detailed properties of the low-metallicity ISM in dwarf galaxies.

2 Radial gas distributions in nearby galaxies

While relations between distributions and densities of gas and star formation in galaxies are of great importance, it is highly instructive to assess the distribution of the atomic and molecular gas in galaxies alone, which ultimately provide the raw material for star formation. The availability of

Table 1 The galaxy sample. Shown are distance, inclination, position angle, as well as the optical radius r_{25} (adopted from Leroy et al. 2013).

Galaxy	Dist. [Mpc]	Incl. [°]	P.A. [°]	r_{25} [']	r_{25} [kpc]
NGC 0337	19.3	51	90	1.5	10.6
NGC 0628[B08, B10]	7.2	7	20	4.9	10.4
NGC 0925[B10]	9.1	66	287	5.4	14.3
NGC 2403[B10]	3.2	63	124	7.9	7.4
NGC 2841[B10]	14.1	74	153	3.5	14.2
NGC 2903[B10]	8.9	65	204	5.9	15.2
NGC 2976	3.6	65	335	3.6	3.8
NGC 3049	19.2	58	28	1.0	2.7
NGC 3184[B08]	11.8	16	179	3.7	12.7
NGC 3198[B10]	14.1	72	215	3.2	13.0
NGC 3351[B10]	9.3	41	192	3.6	10.6
NGC 3521[B08, B10]	11.2	73	340	4.2	12.9
NGC 3627[B10]	9.4	62	173	5.1	13.8
NGC 3938	17.9	14	15	1.8	6.3
NGC 4214	2.9	44	65	3.4	2.9
NGC 4254	14.4	32	55	2.5	14.6
NGC 4321	14.3	30	153	3.0	12.5
NGC 4536	14.5	59	299	3.5	14.9
NGC 4559	7.0	65	328	5.2	10.7
NGC 4569	9.86	66	23	4.6	26.5
NGC 4579	16.4	39	100	2.5	15.0
NGC 4625	9.3	47	330	0.7	1.9
NGC 4725	11.9	54	36	4.9	13.2
NGC 4736[B08, B10]	4.7	41	296	3.9	5.3
NGC 5055[B08, B10]	7.9	59	102	5.9	17.3
NGC 5194[B08, B10]	7.9	20	172	3.9	9.0
NGC 5457[B10]	6.7	18	39	12.0	25.8
NGC 5713	21.4	48	11	1.2	9.5
NGC 6946[B08]	6.8	33	243	5.7	9.8
NGC 7331[B10]	14.5	76	168	4.6	19.5

[B08] Galaxy sample from Bigiel et al. (2008) (Sect. 4.1).
[B10] Galaxy sample from Bigiel et al. (2010a) (Sect. 4.2).

the sensitive, extended and high-quality observations from THINGS and HERACLES (Walter et al. 2008; Leroy et
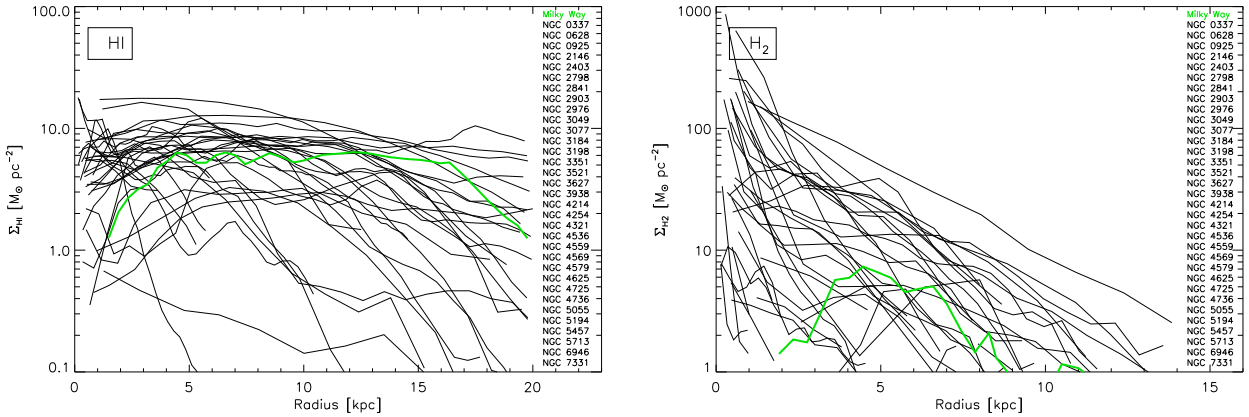
Fig. 2 Azimuthally-averaged radial profiles of the atomic gas (H I, *left*) and molecular gas (H$_2$, *right*) distributions in nearby spiral galaxies. The galaxy sample is listed in the plots. H I and H$_2$ show fundamentally different distributions; the H I profile is often quite flat, while the H$_2$ declines exponentially. The Milky Way (in green) has a rather typical H I and H$_2$ profile.

al. 2009), as well as the ability to stack individual CO spectra to trace the molecular gas out to the edge of the optical disk in galaxies (Schruba et al. 2011), are key requirements for this project, presented in detail in Bigiel et al. (2012). Radial profiles are an excellent means to average out azimuthal variations and focus on the general radial trend of these gas distributions. Such profiles are constructed by sampling the H I and H$_2$ intensity maps of our sample (compare Fig. 1) with a series of tilted rings, matching the inclination and position angle of the disks.

The resulting H I and H$_2$ profiles, i.e. gas surface density Σ_{gas} vs. radius, are shown in the left and right panel of Fig. 2, respectively. They contain a factor of 1.36 to account for the contribution from helium and are corrected for inclination. It is clear from these plots that the warm, atomic hydrogen gas shows substantially different distributions compared to the cold, molecular, star forming gas.

The H I profiles are generally relatively flat and show quite a bit of scatter. However it is evident that the bulk of profiles falls just below $\sim 10\,M_\odot\,pc^{-2}$ for radii $r < 12\,kpc$. Above this H I surface density, the ISM becomes primarily molecular (for near solar-metallicity galaxies, see Martin & Kennicutt 2001; Wong & Blitz 2002; Leroy et al 2008; Bigiel et al. 2008). Many of the interacting galaxies or cluster members have truncated profiles which decrease steeply. Many galaxies show a more or less pronounced depression in the centers. These central "H I holes" are usually regions where the ISM is predominantly molecular (the H$_2$/H I ratio increases roughly exponentially with decreasing radius, e.g., Leroy et al. 2008; Bigiel et al. 2008). For comparison we show the Milky Way H I profile in green, which agrees nicely with the overall trend: H I-deficient in the center and relatively flat throughout at $\Sigma_{HI} \approx 5$–$7\,M_\odot\,pc^{-2}$.

The H$_2$ profiles in the right panel show quite different behaviour: most of them decline exponentially where the scale length varies among the different galaxies, i.e. some profiles are steeper than others. For many galaxies, the H$_2$

surface densities rise steeply in the inner parts (see also Regan et al. 2001). Even on the spatial scales probed here (many square kpc), some galaxies reach surface densities of many $100\,M_\odot\,pc^{-2}$ in the inner parts, quite similar to what is observed in starburst galaxies (e.g., Kennicutt 1998). The Milky Way profile (green) also declines roughly exponentially from $r \approx 5\,kpc$ on outward, but shows a depression at smaller radii. It appears quite typical compared to the other galaxies.

The H I and H$_2$ profiles can be combined to obtain the total gas distribution in our sample galaxies. These profiles are shown in the left panel of Fig. 3. One finds that the combination of the relatively flat H I profiles and the exponential H$_2$ profiles leads to relatively coherent total gas profiles for many of the galaxies compared to the H I or H$_2$ profiles alone. An exponential fit to running means (red line and red points, respectively) shows that the fit is a good characterization of the average trend, excluding the centers with strong molecular gas excesses. The scatter (red error bars) remains below a factor of two at all radii. The total gas profiles cluster at surface densities between a few and a few times $10\,M_\odot\,pc^{-2}$ between $r \approx 2$–$12\,kpc$. The Milky Way profile again appears quite typical and falls right in the middle of the bulk of the profiles.

It turns out that by scaling both axes the right way, one can reduce the scatter among the profiles much further. First, one can remove differences in the physical sizes of the individual galaxies by normalizing the x-axis by the size of the stellar disk, i.e. the optical radius r_{25} (defined as the 25 mag arcsec^{-2} B-band isophote). Second, there appears to be a natural scale of the gas distributions in spiral galaxies, given by at which radii the ISM turns from being primarily atomic (outer parts) to begin primarily molecular (inner parts). This "transition radius" is measured for each galaxy and is used to scale the y-axis. Based on the observation that the mid-plane hydrostatic pressure appears to play an important role for the conversion of atomic to
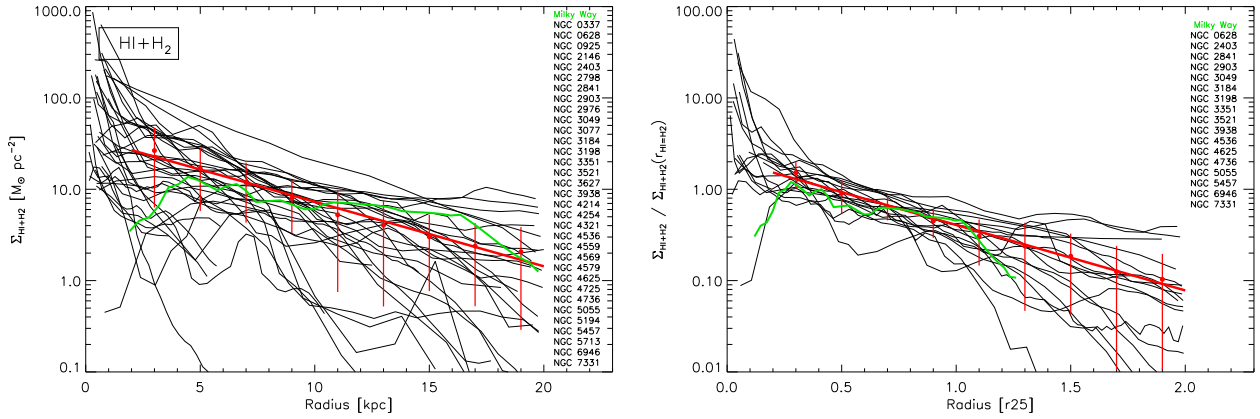
Fig. 3 Azimuthally-averaged radial profiles of the total gas (H I + H$_2$, *left*) and when applying additional scalings to both axes to reduce the scatter (*right*). The resulting fit (in red) describes the galaxy sample well and depends primarily on the size of the *stellar* disk.

molecular gas in galaxies (e.g., Elmegreen 1989; Blitz & Rosolowsky 2004; Leroy et al. 2008), this transition occurs at similar *stellar* surface densities (typically around 81 M$_\odot$ pc^{-2}, Leroy et al. 2008). This hints at the extent of the stellar disk playing an important role for the gas distributions in galaxies, which we will address in more detail below.

The right panel in Fig. 3 shows the profiles with both scalings applied and furthermore with all galaxies showing signs of interactions or cluster members removed, to focus on the relatively undisturbed gas profiles only. Clearly the scatter is dramatically reduced; it is less than 40 % across the optical disks (i.e., $r < r_{25}$) and even at large radii remains below ~ 80 %. The ensemble represents a tight, well-constrained distribution (compare the exponential fit shown by the red line) with deviations in the centres and flaring at large radii.

One can integrate this "universal" neutral gas profile in nearby disk galaxies to obtain the total gas mass $M_{\rm gas}$, which will only depend on the transition surface density and r_{25}:

$$M_{\rm gas} = 0.31 \times 2\pi \times 2.1 \times \Sigma_{\rm trans} \times r_{25}^2 \,. \tag{1}$$

$\Sigma_{\rm trans}$ does not vary dramatically from galaxy to galaxy, but $(r_{25})^2$ varies over two orders-of-magnitude in our sample. Thus, one should be able to use the size of the *stellar* disk to predict the total gas mass of nearby spiral galaxies. This is shown in Fig. 4 where we plot the predicted gas mass from r_{25} and Eq. (1) versus the gas mass as measured from the observations. We find that we can indeed use the size of the stellar disk to predict the gas mass to within a factor of two (indicated by the dashed lines).

The self-similarity of the radial gas distributions for disk galaxies and the important role of the size of the stellar disk for the total gas mass raise a number of intriguing questions. First, it would be interesting to see if these findings hold in other environments, e.g. in lower-metallicity environments, dwarf or elliptical galaxies, where recent studies
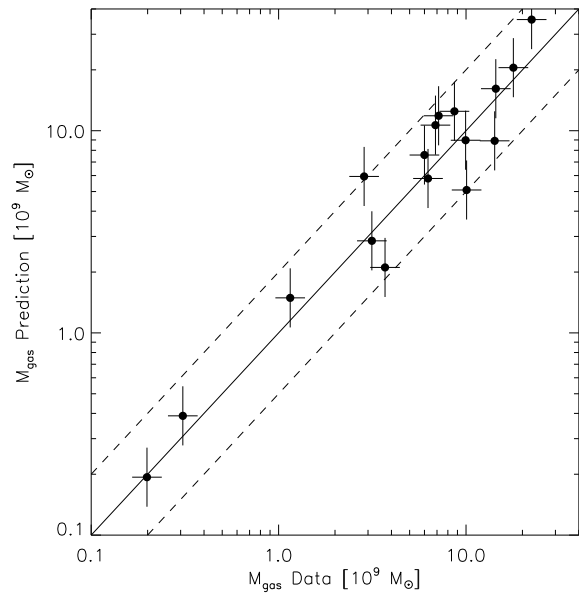

Fig. 4 Comparison of the total gas mass from the observations and as predicted from the fit in Fig. 3 (Eq. 1) and the size of the stellar disk r_{25}. The fit allows to predict the total gas mass of the spirals to better than a factor of two.

reveal quite substantial amounts of atomic and molecular gas (e.g., Young et al. 2011; Serra et al. 2012). Second, why these radial profiles are so self-similar in undisturbed spiral galaxies remains an intriguing question. Star formation in these disks should deplete most of the molecular gas in only about 2 Gyr (e.g., Bigiel et al. 2008, 2011) so that this gas must be replenished. Given that most of the star formation activity occurs within $\sim 0.4\, r_{25}$ (e.g., Leroy et al. 2008), it seems unlikely that gas of external origin falls onto the disk preferentially in the inner parts. If the replenishment happens primarily via gas flows through the disk (compare Sect. 3), it seems hard to understand how the gas distributions can be regulated to be so similar given the range of galaxy types and morphologies covered by our sample. This

universality should be reproduced by cosmological simulations including gas physics and chemistry, which may shed more light on the important processes regulating the gas distribution in galactic disks.

3 Radial gas flows in the disks of nearby spiral galaxies

As pointed out in Sect. 2 above, given the short observed depletion time of of ~ 2 Gyr of molecular gas in the inner parts of galaxies, where most of the star formation takes place, new material must be transported to the inner parts in order to sustain the star formation activity.

One could imagine different mechanisms to provide this material, such as external accretion, high-velocity clouds, tidal interactions or material which is expelled from the disk and re-accreted (e.g., see review by Sancisi et al. 2008). A fair number of nearby disks galaxies already contain significant reservoirs of H I, enough in some cases to sustain the currently inferred star formation rate for up to a Hubble time (e.g., M 83, Bigiel et al. 2010). In that case it needs to be transported towards smaller radii to fuel star formation in the inner parts. This defines the focus of our study, where we are looking for signatures of radial gas flows through the disks of galaxies. We use the high-resolution, sensitive observations in the THINGS data set to look for such signatures. These results will be presented in Schmidt et al., in prep.

The existence of inflows is also predicted by simulations. One very recent and comprehensive study by Marinacci et al. (2014) tracks the detailed evolution of eight Milky Way sized dark matter halos within a cosmological framework to $z = 0$ while including a complex model for baryon physics. The resulting galaxies resemble observed present day spiral galaxies in many ways: They are disk-dominated and show the right bulge-to-disk ratios, nearly exponential surface densities and realistic star formation histories.

These simulations also yield a full kinematic model of the galaxies and their halos. All of their simulated objects show substantial inflow of cold gas which settles onto the galactic plane outside the stellar disk and then radially moves inward. Above and below the stellar disk, inflow is usually prevented by an outward directed galactic wind.

This illustrates that radial inflow should be a relatively common phenomenon in the gas disks of spiral galaxies. The availability of a state-of-the-art data set like THINGS (Sect. 1) allows us to look for signatures of such non-circular motions directly, which would support the indirect expectations from depletion time considerations or morphological indications. Our project is thus to look for large-scale or galaxy-wide radial gas motions by a purely kinematic analysis of the velocity fields of a sample of nearby galaxies.
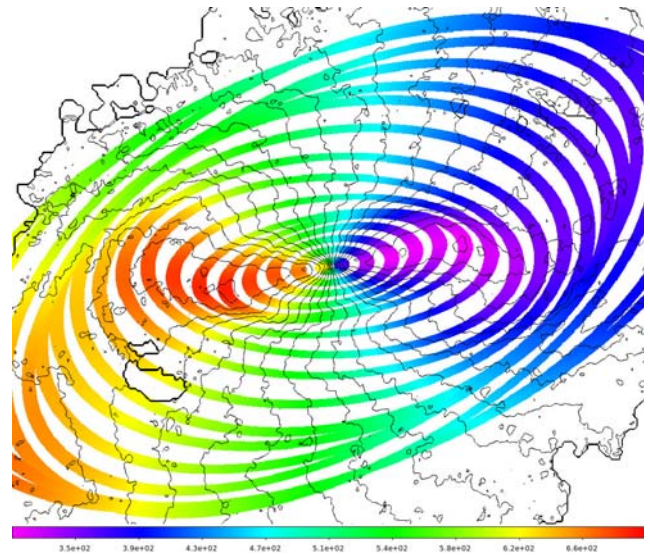

Fig. 5 Illustration of a tilted ring fit to the velocity field of NGC 5055. For better visualization only every second ring is shown. The colour scale represents the velocity relative to the barycentre of the solar system in km s^{-1} and overplotted in black are iso-velocity contours of the data. NGC 5055 has a warped disk, but it is clearly visible how the rings follow the changing inclination and position angle.

3.1 Theory and methodology

The general approach adopted to derive radial profiles (e.g., rotation curves) from a two-dimensional velocity field is known as a "tilted ring fit". The basic idea is to fit the velocity field with circular annuli with varying inclination and position angle. An illustration of this process is shown in Fig. 5.

The observed quantity is the line-of-sight velocity V_{los}. For each ring, it is related to the rotational and – particularly relevant for our study – the radial velocity in the following way:

$$V_{\text{los}} = V_{\text{sys}} + V_{\text{rot}} \sin i \cos \theta + V_{\text{rad}} \sin i \sin \theta. \quad (2)$$

Here V_{sys} denotes the systemic velocity of the galaxy, i is the inclination of each ring, and θ the azimuthal angle which is part of a polar coordinate frame defined within the plane of the ring. The origin of θ is defined by the position angle (PA), the apparent direction of the major axis. The disk is assumed to be thin so that motions perpendicular to the plane of the galaxy are neglected.

This method (though without considering the radial motion term) was established by Begeman (1987) to derive rotation curves of galaxies but was later used and extended by other authors (see below). Often a harmonic expansion of V_{rad} and V_{rot} with respect to θ is performed, which leads to the following relation for V_{los}:

$$V_{\text{los}}(R, \theta) = V_{\text{sys}} + \sin i \Big[c_0 + \sum_{k>0} s_k \sin(k\theta) + c_k \cos(k\theta) \Big]. \quad (3)$$
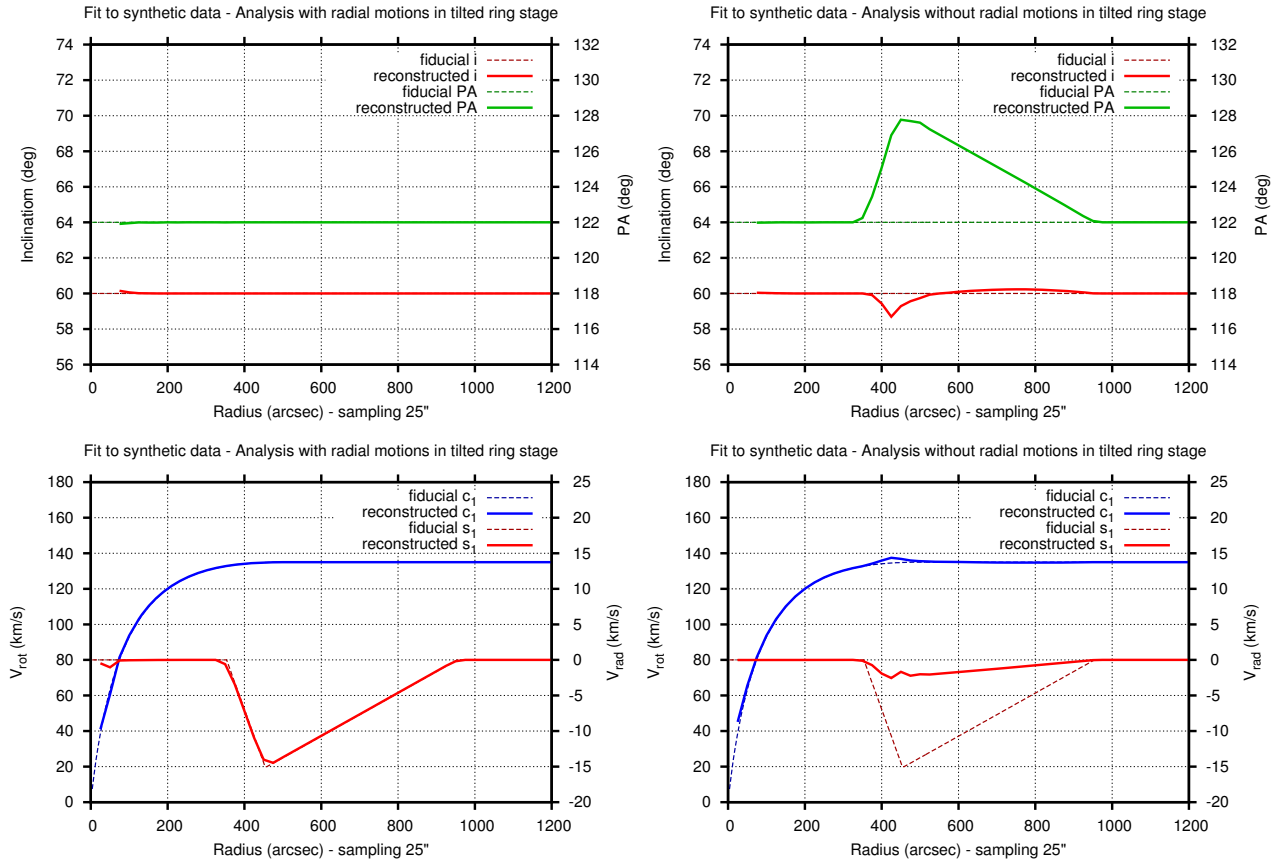
Fig. 6 Different fitting procedures applied to a synthetic velocity field, roughly resembling that of NGC 2403. In each plot the input values used to create the synthetic velocity field are shown as thin dashed lines. *Left*: These plots show the results derived by a fitting scheme in which the radial motions are fitted simultaneously with the ring geometry (our approach). The input values are recovered perfectly. For i, PA, and $V_{\rm rot}$ input values and fit results are indistinguishable. For the s_1 component the plot shows very minor deviations. *Right*: Here we show the results of a fitting scheme in which the ring geometry is determined without taking radial motions into account (as is often the case). During the initial tilted ring fit the position angle is fitted to a mismatched value (up to $6°$) to compensate for the radial motion. In the subsequent Fourier decomposition only a small fraction of the actual radial inflow is detected. The Fourier decomposition does not lead to correct inflow velocities because of the wrong ring geometry.

This breaks the rotational symmetry and adds more degrees of freedom to the model, but it also makes the reconstruction of the in-plane Fourier components of $V_{\rm rad}$ and $V_{\rm rot}$ from the measured line-of-sight Fourier components (c_k, s_k) non-unique. It also complicates the fitting process itself, in which c_k, s_k, i, and PA are determined.

In former studies (e.g., Schoenmakers et al. 1997; Trachternach et al. 2008) a two-step approach was used. First, a simple tilted-ring model representing a purely rotational axisymmetric velocity field was fitted to the data to determine the geometry of the disk (i, PA). In a second step, the geometry was fixed and the velocity field was decomposed into higher-order Fourier components including radial motions.

However, even if the Fourier components form an orthogonal base, at least the odd-order terms couple to i and PA. It may therefore be problematic to derive the full set of fit parameters in two separate steps. We found that in the first step (tilted ring fit) in particular the position angle tends to compensate for a potential radial velocity component not accounted for in the tilted ring fit. If this geometry is subsequently used in a second step to derive the full velocity field,

the radial velocity will not be determined correctly as it is based on a wrong geometry. This can at least in some cases prohibit the detection of significant radial gas flows. We found this scenario using THINGS H I data for NGC 2403 (discussed in more detail below), but could also accurately reproduce this effect using synthetic velocity fields (shown in Fig. 6).

It is thus necessary to fit all parameters simultaneously in a single step in order to recover more reliable fit parameters. Unfortunately, this procedure allows to include Fourier components only up to the second order. Specifically, the c_3 and i terms are highly degenerate, which prohibits a simultaneous fit of these two parameters and makes a proper measurement of c_3 impossible in most cases.

Summarized, our approach is thus to fit simultaneously (s_1, c_1, s_2, c_2) as well as i and PA for each tilted ring. The center coordinates (X_C, Y_C) and systemic velocity are determined in advance and are kept fixed for all rings. We verified the robustness of our fitting scheme by applying it to a large number of synthetic velocity fields, where we correctly reconstruct the input parameters.

3.2 NGC 2403: a case study

We apply our improved simultaneous fitting scheme to several extended disk galaxies from the THINGS survey. NGC 2403 is the best and most promising target, because it has a very flat and smooth H I disk without major disturbances. This makes it an ideal target to look for non-circular flows.

The results are shown in Fig. 7: We find clear evidence for radial inflow. The radial direction of the gas motion can be inferred from the rotation direction of the galaxies, which we determine from visual images, especially from the more pronounced appearance of dust filaments on the near side of the disk. By combining this information with the velocity field, it is clear that the radial motion is indeed inward. The derived radial velocity is negative almost across the entire disk corresponding to inflow of at least a few $km\,s^{-1}$. The most significant radial flow is visible between $400''$ and $900''$. The highest H I mass flux ($3\,M_\odot\,yr^{-1}$, contribution from helium is not included in this section) is observed at a radius of $450''$, corresponding to $\sim 7.6\,kpc$ at a distance of $3.5\,Mpc$. The inflow then declines almost linearly towards larger radii.

The star formation rate for this galaxy given in Leroy et al. (2008) is only $0.38\,M_\odot\,yr^{-1}$. This is of the same order as our minimum inflow rate, but nearly an order of magnitude lower than our maximum inflow rate of $3.5\,M_\odot\,yr^{-1}$. Most of the star formation activity happens in the inner part of the galaxy, well inside the peak inflow radius. This lends support to the picture of gas transport, with high velocities preferably at larger radii, and subsequent consumption by star formation in the inner parts.

3.3 Extension to other galaxies

The application of our method to other THINGS galaxies gives a more inhomogeneous picture. To provide some examples, for NGC 3198 and NGC 6946 as well as to some degree for NGC 2903 and NGC 7331 we also find radial inflows. But other spirals like NGC 2841 and NGC 925 show no signs of inflow but instead significant outflow ($> 1\,M_\odot\,yr^{-1}$). at large radii if we determine the receding and approaching sides correctly.

The mass flow we detect is usually not constant with radius but varies. In many cases we see the highest inflow rates at intermediate radii and a weak signal in the outermost parts. Such pattern can obviously not represent a steady state. For example for NGC 3198, we find a maximum inflow rate of $1.5\,M_\odot\,yr^{-1}$ at $400''$ and less than $0.5\,M_\odot\,yr^{-1}$ across the outer disk. Therefore, the H I inventory of $\approx 2.2 \times 10^9\,M_\odot$ outside of $400''$ would be depleted on a time scale of 1 to 2 Gyr. Also, many of the galaxies in which we detect inflow, the inflow rate is significantly higher than the star forming rate. Possible interpretations may be that additional internal streaming motions, re-accreted gas expelled from the disk ("galactic fountain")
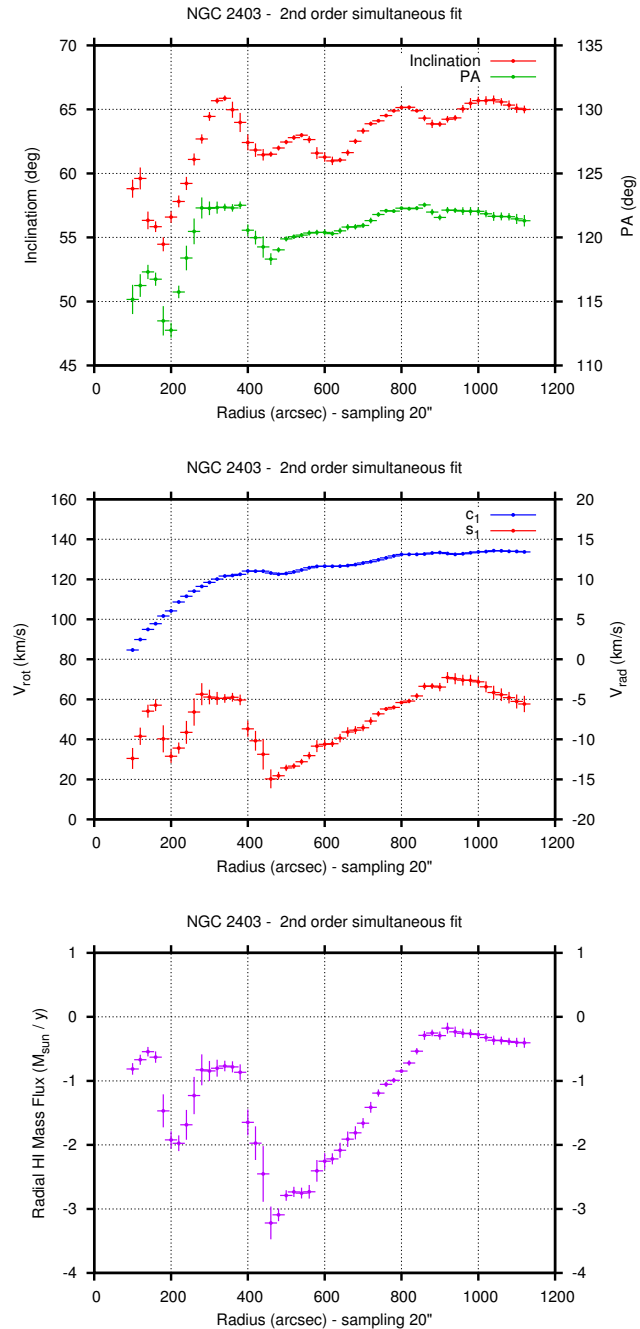

Fig. 7 Disk geometry and Fourier parameters for NGC 2403. The galaxy shows a smooth and unperturbed disk, position angle and inclination show only minor variations. The radial velocity shows a very distinct signature between $400''$ and $900''$ with a peak inflow velocity of $15\,km\,s^{-1}$. Using the total H I column density maps, this can be converted to a H I mass flow of up to $3\,M_\odot\,yr^{-1}$. The inflow almost stops inside of $400''$ and then shows a second smaller feature at $200''$. For very large radii we find inflows of about $0.5\,M_\odot\,yr^{-1}$.

or H I gas from the intergalactic medium is accreted in occasional events and temporarily leads to higher mass flow rates. However, the fact that we find this scenario for many galaxies with inflow motions means that all or some of these processes must play an important role supplying the galaxies with additional gas.

NGC 5055 has a relatively tilted and warped disk in the outskirts, for which we find some outward motion. However, warped, possibly flaring, outer disks are difficult to model with tilted rings. The appearance of the NGC 5055 disk could be a direct result of a recent minor merger, for which a tidal stream was reported by Chonis et al. (2011).

In general, we find that the large spiral THINGS galaxies usually have complex structures and simple, unperturbed disks are the exception. An extreme case is NGC 3521, which shows extremely perturbed kinematics. Our methodology is clearly not able to model such large asymmetries and irregularities in the velocity field along with locally varying and possibly out-of-plane motions of the gas. For NGC 3198 and NGC 7331 we find indications that inflow may happen more localized on smaller scales in azimuthal angle than we can resolve.

Many of the galaxies in our sample show at least some variation in inclination or position angle with radius. An analysis that should be applied to large parts of a galactic disk and especially to the outskirts has to be able to adapt to warps and perturbations to get the velocity terms right. Assuming an azimuthally only slowly varying velocity field – as we did – is borderline: For unperturbed galaxies this approach yields good results, but many galaxies have streams or other more localized features, which we sometimes see signatures of but cannot resolve or interpret with our method.

While including higher-order Fourier terms to increase azimuthal resolution is possible formally, the system of equations becomes degenerate: there are too few observables to be able to uniquely reconstruct radial and rotational velocities.

4 Gas and star formation rate scaling relations in nearby galaxies

A key question in studies of the interstellar medium in galaxies is how its properties are related to the observed star formation activity. More specifically, understanding the role of ISM parameters (composition, physical properties) but also galaxy dynamics in driving the star formation efficiency across galactic disks is key in the context of galaxy evolution. Particularly important is how "ISM observables", especially gas surface densities, can be connected to the observed SFR. Such relations are central not only for our understanding of the regulatory processes governing star formation on small and large scales, but also as input and a baseline of comparison for simulations of individual galaxies as well as on cosmological scales.

A relationship between the volume densities of atomic gas and stars in the Milky Way was first suggested many decades ago by Schmidt (1959). Kennicutt (1989, 1998) carried out the first comprehensive extragalactic study targeting a large sample of nearby galaxies, normal spirals as well as starburst galaxies, focusing on measurements averaged across galaxy disks. He found a close power-law correlation between the galaxy-average total gas surface density ($\Sigma_{\rm gas} = \Sigma_{\rm HI} + \Sigma_{\rm H2}$) and the galaxy-average SFR surface density ($\Sigma_{\rm SFR}$). Because volume densities are difficult to measure in other galaxies, it has since become standard to study the relationship between gas and star formation via surface densities.

4.1 The gas-star formation relation across the optical disks

With all the new data sets introduced above (Sect. 1) in hand, a matched set of sensitive, high spatial resolution maps of atomic gas, molecular gas and star formation tracers for a large sample of nearby galaxies became available. The resolution of the maps allows hundreds of independent measurements per galaxy (roughly 1 kpc-sized "pixels"), leading to significantly improved statistics and the ability to isolate regions with specific physical conditions.

In Bigiel et al. (2008) we combined the data obtained from sampling our intensity maps (compare Fig. 1) on ~ 1 kpc scales to compare the surface densities of atomic gas, molecular gas and the star formation rate across the optical disks ($r < r_{25}$) for a sub-sample of 7 spiral galaxies (marked in Table 1). Figure 8 shows the results of this analysis: the left panel shows $\Sigma_{\rm HI}$, the middle panel $\Sigma_{\rm H2}$, and the right panel $\Sigma_{\rm gas} = \Sigma_{\rm HI} + \Sigma_{\rm H2}$ (not including the contribution from helium) versus $\Sigma_{\rm SFR}$ (derived from a combination of far UV and 24 μm emission). Far UV emission is photospheric emission from mainly O and B stars with a typical age of ~ 20–30 Myr and serves as a tracer for recent, dust-unobscured SF. The 24 μm emission comes from dust heated by mainly young stars so that the combination of the two tracers provides a "complete" tracer of the SFR, well matched to other calibrations, e.g., using extinction-corrected Hα emission (compare, e.g., Leroy et al. 2008, 2012 for an in-depth discussion).

One finds that H I and H$_2$ show quite distinct behaviors: the atomic gas shows no clear correlation with the SFR, whereas the molecular gas exhibits a strong correlation. For H I + H$_2$ in the right panel one finds that the combined total gas-SFR relation does not follow a single power law. One can distinguish two separate regimes in this plot: at low gas columns the ISM is H I dominated (steep relation) and at higher gas columns (> 10 M$_\odot$ pc^{-2}) the ISM is H$_2$ dominated (roughly linear correlation).

The H$_2$ distribution in the middle panel can be characterized with a power law fit, which yields a power law index of $N \approx 1.0$. This can be restated as a constant ratio $\Sigma_{\rm SFR}/\Sigma_{\rm H2}$, which means that on average the SFR per unit

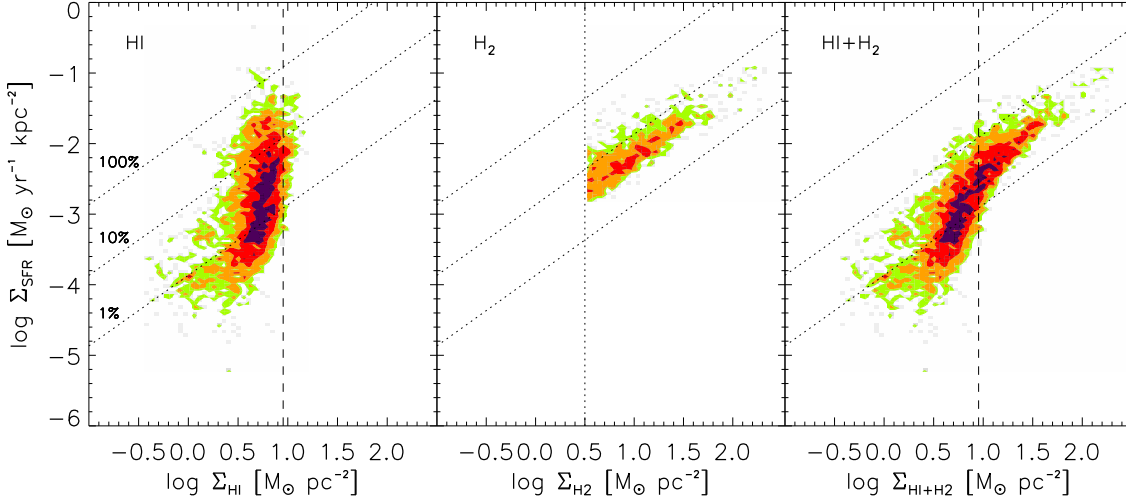**Fig. 8** Σ_{SFR} versus Σ_{HI} (*left*), Σ_{H2} (*middle*), and $\Sigma_{gas} = \Sigma_{HI} + \Sigma_{H2}$ (*right*) for pixel-by-pixel data from 7 nearby spirals at ~ 1 kpc resolution. The contours represent the density of sampling points (pixels), where darker colors indicate a higher density. While the H I shows almost no correlation, the H_2 is strongly correlated with the star formation rate implying an approximately constant H_2 depletion time of ~ 2 Gyr.

H_2 is approximately constant. We searched for correlations between this "star formation efficiency" Σ_{SFR}/Σ_{H2} and a number of environmental variables, such as dynamical time, mean hydrostatic pressure in the ISM, gas or stellar surface density, galactocentric radius (as proxy for other radially varying quantities such as metallicity), but only marginal or no variation at all was found (Leroy et al. 2008, 2013). Many of these quantities in turn did correlate strongly with the molecular gas fraction (Σ_{H2}/Σ_{HI}). Thus, one can combine these findings and conclude that in nearby spiral galaxies the average efficiency of star formation in the molecular gas is fairly constant (as is its inverse, the H_2 depletion time $\Sigma_{H2}/\Sigma_{SFR} \approx 2.0$ Gyr), while the abundance of molecular gas is a strong function of conditions in the ISM as well as of galactic dynamics.

Over the years numerous studies have been carried out probing the relation between gas and SFR surface densities in other galaxies. They focus on different galaxies, use different SFR tracers, and probe different scales (galaxy averages, radial profiles, pixel-by-pixel sampling comparable to our approach or selected apertures, e.g., centered on individual H II regions). It is thus instructive to compare these measurements directly in an aggregate plot (note that we do adjust the CO-to-H_2 conversion factor when deriving Σ_{H2} and the IMF when deriving Σ_{SFR} to match our assumptions, but leave the data unchanged otherwise). Figure 9 shows this compilation; the references to the various data sets are provided in the plot legend and further details can be found in Bigiel et al. (2011).

Figure 9 nicely illustrates that while individual measurements and galaxies may deviate from the overall trend and scatter is substantial, all these diverse measurements occupy a well-defined regime in Σ_{SFR}-Σ_{H2} space. The black points show a running median and 1σ scatter representing our own
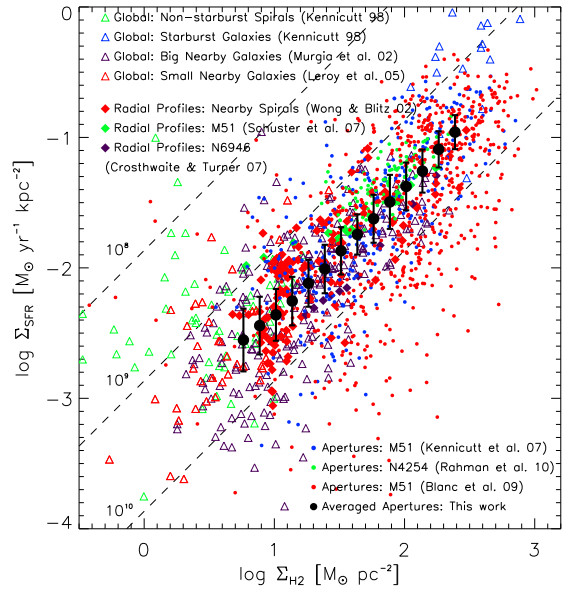

Fig. 9 Σ_{SFR} and Σ_{H2} for a wide compilation of literature measurements referenced in the legend. Despite different methodology and tracers, the diverse data sets occupy a well-defined regime in this plot. We compare these measurements to our own data (running median in black), which is in excellent agreement with the general trend and implies an average H_2 depletion time of ~ 2 Gyr.

measurements (similar to the middle panel in Fig. 8 but now extended to 30 spiral galaxies rather than 7, compare Table 1). One finds that these averages represent an excellent characterization of the mean trend of these different data sets, re-confirming the conclusion of an approximately linear power law relationship between Σ_{SFR} and Σ_{H2}. This comparison also implies that this result is largely robust with respect to the choice of tracers or experimental setup.
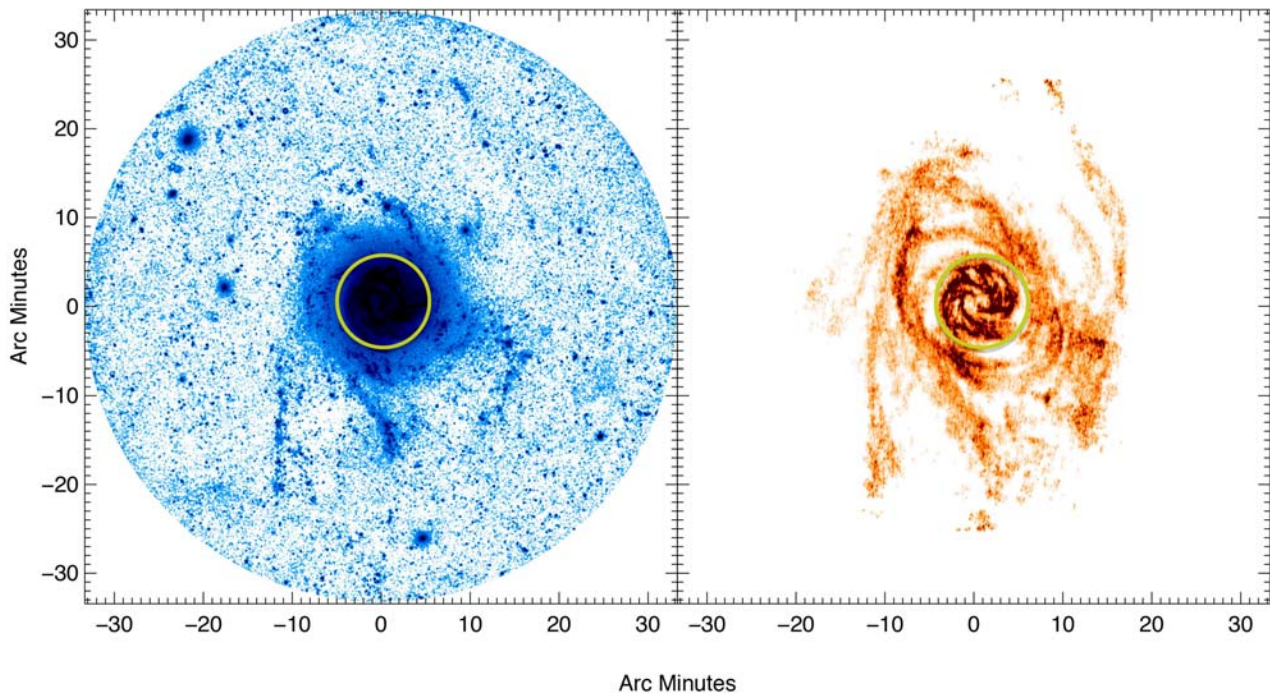
Fig. 10 Far UV emission from GALEX (*left*) and H I emission from THINGS (*right*) for the spiral galaxy M 83 (Bigiel et al. 2010b). The green circle indicates the extent of the optical disk (r_{25}). One finds atomic gas and widespread star formation out to four times the optical size of the galaxy. There is excellent agreement between the UV emission from massive stars and the H I distribution out to large radii.

4.2 Star formation beyond the optical disks

For many nearby spiral galaxies, the H I distributions reveal atomic gas out to many times the optical radius (Fig. 10). In particular GALEX UV observations have revealed widespread SF in the outer parts of many galaxies (e.g., Thilker et al. 2005; Gile de Paz et al. 2007; Bigiel et al. 2010b). The conditions in these outer galaxy disks are, however, distinctly different from those in the inner parts of galaxies: less abundant heavy elements, less dust, and lower stellar and gas surface densities should make these environments less favorable for gas to efficiently cool and form stars. It is thus an interesting exercise to compare scaling relations between gas and SF in the outer disks to those obtained for the optical disks of galaxies presented above.

We show this comparison in Fig. 11. The open contours show pixel-by-pixel sampling data of Σ_{SFR} versus Σ_{gas} for a sample of 14 spiral galaxies on scales of about 1 kpc from Bigiel et al. (2010a) (compare Table 1). SFRs are estimated from GALEX far UV emission and Σ_{gas} is estimated from H I emission alone, assuming a negligible contribution from molecular gas on $\sim$ kpc scales in the low-metallicity environment of outer galaxy disks.

For comparison, we show the distribution obtained from the optical, star-forming disks shown in the right panel of Fig. 8 from Bigiel et al. (2008). In the outer disks (open contours, black points show a running median), Σ_{SFR} scales with $\Sigma_{gas} = \Sigma_{HI}$, though the scatter in Σ_{SFR} at any given H I column density is quite large. Compared to the inner parts

(filled contours), this is a notable difference as we found no significant correlation between Σ_{SFR} and Σ_{HI} at small radii (compare Fig. 8).

The distribution we observe for the outer disks of galaxies suggests that the amount of available H I seems to be a key parameter regulating H_2 and subsequent star formation. More H I implies on average higher SFRs at large radii. This is a significant difference compared to the inner parts, where abundant H I is available everywhere as raw material for cloud and star formation. The large scatter for the outer disk data implies though that other properties must play an important role in regulating the SFR at large radii as well.

Many physical conditions important for the H I-to-H_2 conversion vary substantially across the inner parts of galaxies (pressure, stellar surface density, metallicity, compare Sect. 4.1), while Σ_{HI} remains approximately fixed. In the outer parts, however, Σ_{HI} varies while other environmental conditions show comparatively little variation (e.g., dust abundance or metallicity). This implies that while Σ_{HI} is not a critical quantity for SF in the inner parts, it plays an important role at large radii. This is illustrated in Fig. 10 above, where one finds a tight correlation between abundant H I and star formation traced by UV emission in the spiral galaxy M 83. For this galaxy, the H I depletion time is about a Hubble time and thus much larger than the H_2 depletion time scale of ~ 2 Gyr (Sect. 4.1). In contrast to the inner parts, this suggest that in the outer disks of galaxies H_2 formation or cloud assembly is the limiting process for SF.
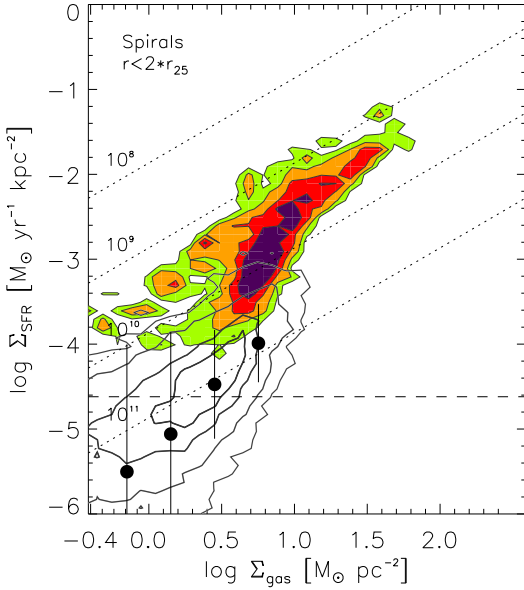
Fig. 11 Σ_{SFR} versus Σ_{gas} from sampling our data with 1 kpc pixels for the outer (open contours, running median and 1σ scatter in black) and inner (filled contours from Fig. 8) parts of nearby spiral galaxies (Sect. 4.1) from Bigiel et al. (2010a). Star formation proceeds much less efficiently at large radii.

Moving from the outer disks to intensely star-forming environments, there is good reason to believe that in this regime the scaling relation between Σ_{SFR} and $\Sigma_{\mathrm{gas}} = \Sigma_{\mathrm{H2}}$ (because $\Sigma_{\mathrm{H2}} \gg \Sigma_{\mathrm{HI}}$) also deviates from the proportionality observed across the star forming disks of galaxies. Observations indicate an increasing star formation efficiency with increasing molecular gas column density, translating into a significantly steeper than linear power law relationship (explaining the often measured power-law index of around $N \approx 1.5$, e.g., Kennicutt 1998; Gao & Solomon 2004; Bouché et al. 2007). This is observed for H_2 surface densities above $\sim 100\ \mathrm{M_\odot\ pc^{-2}}$, which are typically found in more vigorously star forming systems, like starburst galaxies, LIRGs and ULIRGs, which convert molecular gas into stars much more efficiently, often triggered by galaxy interactions.

While there is some consensus emerging on how different galaxies (or different parts of galaxies) populate the Σ_{SFR}-Σ_{gas} parameter space, it is clear that a simple power-law cannot adequately explain the observed data distribution. Nonetheless, such scaling relations provide a baseline of comparison which simulations should be able to reproduce to test their respective implementations of star formation, gas physics and chemistry, feedback, etc. It is also becoming increasingly clear that the gas surface density alone is not sufficient to predict the SFR within a galactic disk. Other environmental quantities play an important role in setting the molecular gas fraction and thus the amount of cold, dense, star forming gas (e.g., Leroy et al. 2008, in prep.). Looking for and assessing the importance of potential drivers for the molecular gas fraction across galactic

disks, and in particular in different galactic environments, are the next major steps towards a more comprehensive understanding of galactic scale star formation.

5 Properties of the low-metallicity ISM in nearby dwarf galaxies

One key challenge is to extend the studies of star formation rates and efficiencies and how these are linked to the properties of the ISM to lower metallicity environments. These environments are interesting to contrast studies in decent metallicity, Milky Way like disk galaxies to learn about the role of dust and metals in the star formation process, but also because a less enriched ISM resembles in many ways that of galaxies at higher redshift. Nearby dwarf galaxies can be studied at high resolution and their chemically relatively unevolved ISM makes them ideal laboratories to study the properties of the ISM in such an intriguing environment. In particular, dwarfs often show active star formation, which, in light of the low ISM metal content, raises the question of how the ISM can efficiently cool and form stars.

Dwarf galaxies are thus perfect candidates to address fundamental questions such as: How do the physical conditions of star-forming regions vary as a function of the elemental enrichment? What controls the energy balance, heating and cooling in the different (ISM) phases and what shapes the morphology of dwarf galaxies? What are the roles of the different ISM phases in the integrated view of galaxies?

As shown above (Sect. 4.1), star formation in roughly solar-metallicity galaxies appears to be regulated essentially by the molecular gas reservoir (e.g., Bigiel et al. 2008, 2011; Genzel et al. 2012). However CO emission is elusive in low-metallicity environments (due to more efficient photodissociation), while H_2 can efficiently self-shield ("CO-dark gas", see, e.g., Wolfire et al. 2010 or Bolatto et al. 2013 for details). This means that emission from the CO molecule becomes an increasingly poor tracer of the molecular, star forming gas at low metallicity. How efficient SF really is under these very different physical conditions is thus difficult to address with CO observations.

One way to probe the conditions in the ISM at low metallicity is spectroscopy in the far-IR (FIR). The FIR cooling lines, unaffected by dust attenuation, are powerful probes of the star formation activity, linking them directly to the surrounding medium from which these stars are born. They generally arise in H II regions and photodissociation regions (PDRs), which are the interfaces between H II regions and molecular clouds in galaxies. The fine-structure lines [C II] $157\ \mu m$, [O I] $63\ \mu m$ (and [O I] $145\ \mu m$) are important coolants of the dense ($n_{\mathrm{H}} > 10\ \mathrm{cm^{-3}}$) warm ($T \sim 100$–$300\ \mathrm{K}$) neutral ISM and amongst the brightest cooling lines in star-forming galaxies. The [N II] $122\ \mu m$ and $205\ \mu m$ and [O III] $52\ \mu m$ and $88\ \mu m$ lines are tracers of the ionized gas. They are important diagnostics of the FUV flux, gas density, temperature, and filling factor of the

PDR and ionized regions (e.g., Tielens et al. 1985; Kaufman et al. 2006). In combination with the mid-IR (MIR) lines (e.g. [S III] 18.71 μm and 33.48 μm, [Ne III] 15.56 μm, [Ne V] 14.32 μm, [Si II] 34.82 μm, warm H_2 lines and emission from polycyclic aromatic hydrocarbons – PAHs) they provide a complete view on ISM conditions and excitation processes.

In dwarf galaxies, the FIR lines were first detected by the Kuiper Airborne Observatory and the Infrared Space Observatory (ISO) in Local Group and other bright dwarf galaxies only. The brightness of the FIR lines contrasts the faintness of the CO emission, resulting in, e.g., high [C II]-to-CO(1–0) ratios (Madden et al. 2000). Interpreting these observations in terms of excitation led to first evidence of a reservoir of "dark gas", not seen in CO emission but well detected in C^+ (e.g., Poglitsch et al. 1995; Madden et al. 1997). This makes the FIR lines a potentially very useful tool to trace star formation (De Looze et al. 2013), which could be used in particular for high-redshift studies (e.g., with ALMA), and to calibrate the "dark gas" fraction at low metallicity.

The advent of the *Herschel* telescope and the PACS instrument has provided a unique opportunity to study the dust and gas in larger samples of chemically unevolved systems. The *Herschel* Guaranteed Time Key Program "The Dwarf Galaxy Survey" (DGS, Madden et al. 2013) is a 230 hours project which aims to study the dust and gas properties with the PACS (Poglitsch et al. 2010) and SPIRE (Griffin et al. 2010) instruments in a sample of 50 dwarf galaxies. These dwarf galaxies have different morphologies, star formation activities (as high as 25 $M_\odot$ yr^{-1} in Haro 11), and metallicities (down to 1/40 $Z_\odot$ in I Zw 18). All of them are nearby galaxies, no further than 200 Mpc, enabling us to study local variations of key ISM properties and relating them to the observed star formation activity.

5.1 *Herschel* PACS line ratios

The *Herschel* dataset provides unique information on ISM properties. FIR line ratios are important diagnostics of the gas conditions. In the following we present correlations between several FIR tracers to identify empirical trends in the sample, and to link observational trends to global galaxy parameters. The dwarf galaxy sample is also compared to the sample of Brauher et al. (2008), containing a larger variety of galaxies and in particular extending to more metal-rich galaxies, starbursts, and active galactic nuclei.

In Fig. 12 we plot PACS line ratios versus two key quantities: the IRAS band ratio of 60/100 μm, which is an indicator of the dust temperature, and L_{TIR}, which is an indirect probe of the star formation rate. L_{TIR} is commonly used as a proxy for the gas temperature (e.g., Rubin et al. 2009), since it includes all contributions from the dust emission, and in particular the small grains and PAHs, which are the main actors of photo-electric heating.
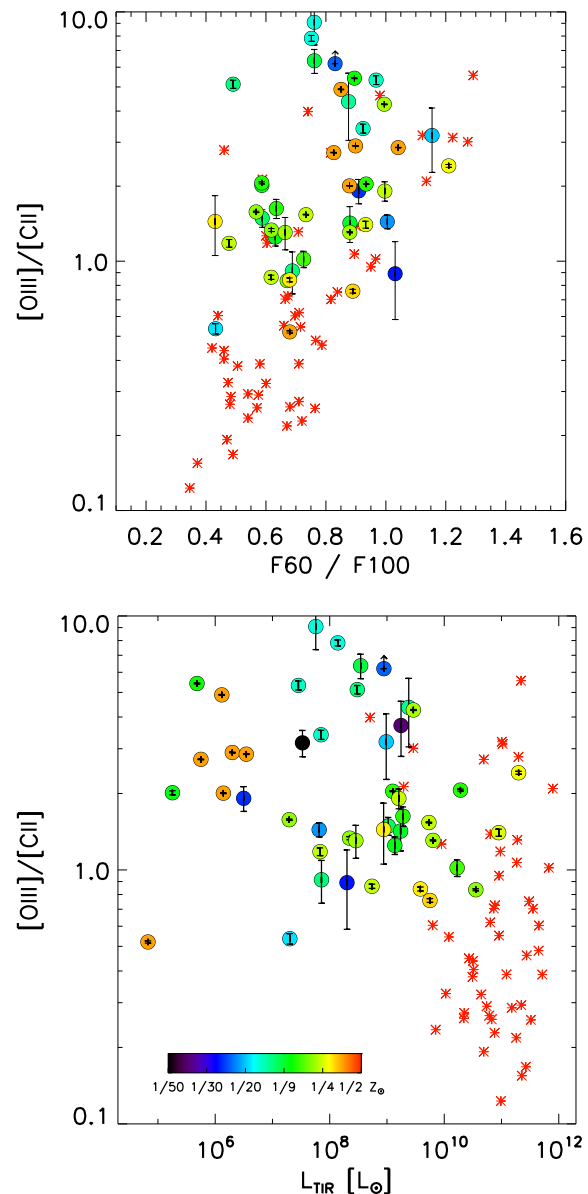

Fig. 12 PACS line ratios: [O III]/[C II] versus 60/100 μm and L_{TIR}. The DGS galaxies are represented by filled circles color-coded by metallicity. We overplot the galaxies from Brauher et al. (2008) with red stars.

5.1.1 [O III] 88 / [C II] 157: H II region versus PDR

Figure 12 shows that the [O III] 88 μm line is very bright in the DGS galaxies and is the brightest line in most cases. This is true – not only locally in extended sources where the peaks of emission are ~ 10 times brighter than the [C II] 157 μm line (e.g. 30 Doradus) – even integrated over full galaxies. The [C II] line is the second brightest FIR line. In compact objects, [C II] often shows a larger spatial extent than the other lines, hinting perhaps towards an important contribution from a diffuse phase.

Values of [O III] 88/[C II] 157 span more than an order of magnitude, from 0.4 to 12, and [O III] is on average 2.1 times higher than [C II]. This is surprising, at first,
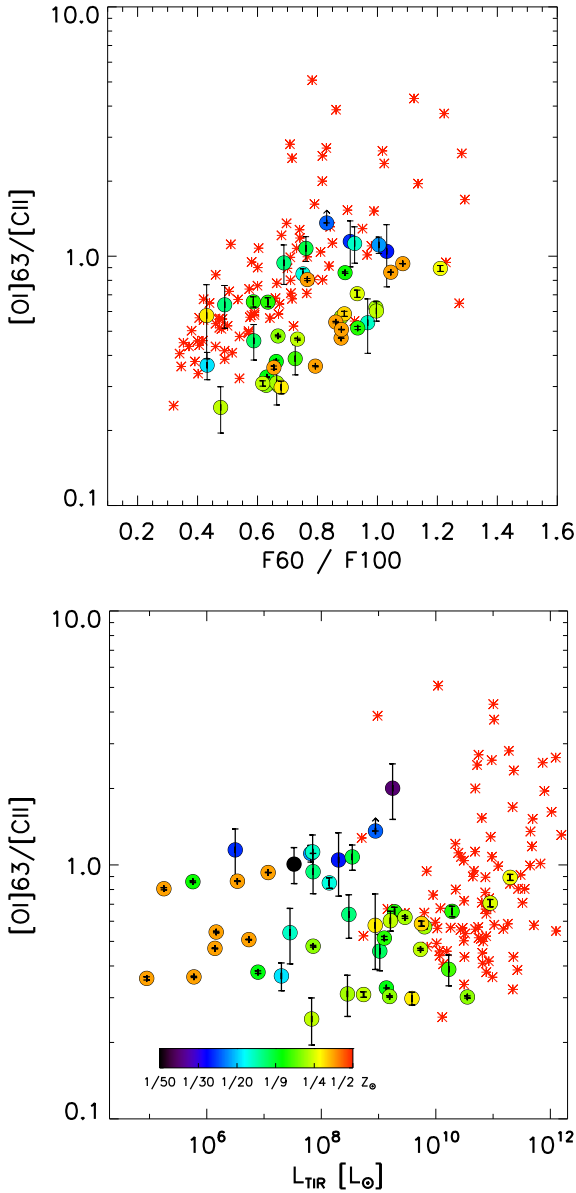
Fig. 13   PACS line ratios: [O I] 63/[C II] versus 60/100 μm and $L_{\rm TIR}$. Same color-coding as in Fig. 12.

Fig. 14   PACS line ratios: [O III] /[N II] 122 versus 60/100 μm and $L_{\rm TIR}$. Same color-coding as in Fig. 12.

as it requires 35 eV photons to create a O^{++} ion while the [C II] is more easily excited (the ionization potential of C^0 is 11.26 eV). Bright [O III] is likely related to the starbursting nature of many of the dwarf irregular galaxies in the DGS. [O III] is furthermore detected over large spatial scales, indicating the presence of low density channels where the UV photons can travel far to excite the gas.

5.1.2   [O I] 63 / [C II] 157: characterizing the PDR

[O I] 63 usually dominates the cooling in resolved PDRs (e.g. the Orion Bar, Bernard-Salas et al. 2012) and we find that it is often brighter than [C II] on peaks of extended sources (e.g. N66 in the SMC). Figure 13 shows that, integrated over galaxy scales, it is on average fainter than [C II],
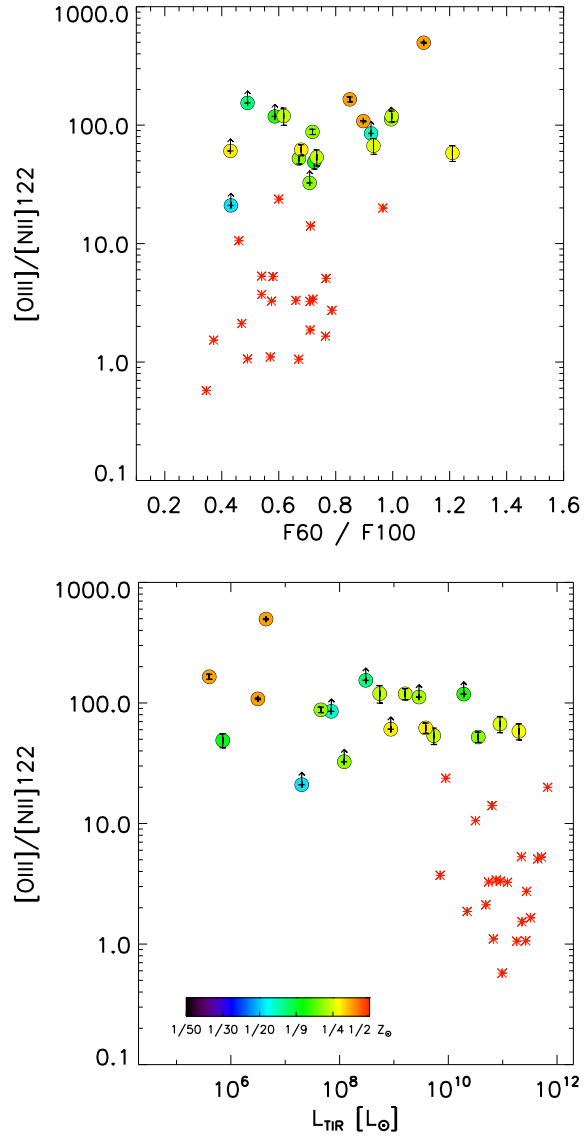
with [O I] 63/[C II] 157 $\sim$ 0.64. The ratio of DGS galaxies falls in the range observed by Brauher et al. (2008), although located in the lower range of their observed [O I] 63/[C II] values.

We see an increase of [O I] 63/[C II] 157 with FIR color for the dwarf galaxies, which is less pronounced than in Brauher et al. (2008) (Fig. 13). Models indicate that this ratio globally increases with density and radiation field (Kaufman et al. 2006), as the critical density and excitation energy of [O I] 63 are higher than for [C II], and therefore higher ratios are expected in compact H II regions. The relatively low ratios of [O I] 63/[C II] 157 observed in dwarf galaxies could be due to (1) optical depth effects on the [O I] 63 μm line, which becomes significantly optically thick for $A_V \geq 5$ (Abel et al. 2007); and/or to (2) a low-density origin of [C II] emitting ionized or neutral gas. We note that [O I] 63/[C II] 157 values are relatively high in the LMC regions, which is

explained by the fact that we have zoomed in on the star-forming sites, where the high densities and strong radiation fields favor emission from [O I] rather than [C II], and we are also missing some extended [C II] emission compared to global values.

5.1.3 [O III] 88 / [N II] 122: gas excitation

The [O III] 88/[N II] 122 ratio is very high in dwarf galaxies, with average value 130. The [O III] 88/[N II] 122 ratio decreases with increasing $L_{\rm TIR}$ and is not correlated with 60/100 μm (Fig. 14). [O III] and [N II] 122 μm have similar critical densities (~ 300–500 cm^{-3}), but different excitation potentials (35.5 and 14.5 eV, respectively). The harder radiation fields present in dwarf galaxies hence favor the excitation of [O III] (and [N III] rather than [N II]). The fact that [O III] and [N II] 122 μm behave similarly with FIR colors may indicate an important contribution of low density ionized gas to these lines, in addition to the compact H II regions.

5.1.4 Photoelectric efficiency

We also analyze the ratio of the [C II] 157 and [O I] lines to $L_{\rm TIR}$, which is a measure of the photoelectric efficiency, provided the main heating source for the [C II] line is the photoelectric effect.

Star-forming dwarf galaxies exhibit generally lower dust abundances due to their lower metallicity, high ionisation parameters and reduced PAH abundances due to the hard radiation fields. Without detailed investigation of the dust properties, this would indicate lower photoelectric efficiencies in dwarf galaxies. However, dwarf galaxies also exhibit enhanced small grain abundances (e.g., Galliano et al. 2003), which contribute to the photoelectric heating. Because of the lower dust content, the mean free path of UV photons is larger, resulting in a UV field dilution over larger spatial scales, which may result in less grain charging. The end result is that we observe a relatively *efficient* photoelectric effect (see also Israel et al. 2011), with observed ([C II] + [O I])/TIR ratios higher in dwarf galaxies than in normal galaxies (Fig. 15).

5.2 Description of the distribution of the ISM phases

The general trends that we observe in the line ratios have implications on the ISM properties of dwarf galaxies, although modeling of individual galaxies is required to recover detailed gas conditions (temperature, density). The FIR lines are globally bright relative to the TIR luminosity, together accounting for a few percent of $L_{\rm TIR}$ – always brighter than the more metal-rich galaxies. This indicates that the gas cooling line intensities are *enhanced on galaxy-wide scales*. When zooming on the active regions of the LMC, line-to-TIR ratios appear higher than for galaxy-integrated values. This confirms that the dwarf galaxies are dominated by emission from their star-forming regions
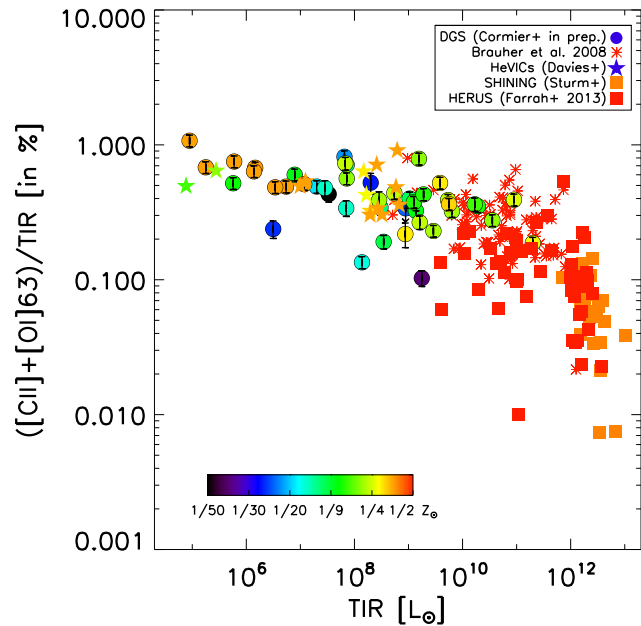

Fig. 15 PACS line-to-TIR ratio: ([C II] 157 + [O I] 63)/TIR versus $L_{\rm TIR}$. Same color-coding as in Fig. 12.

even on galaxy scales. In terms of ISM structure, the high [C II]/TIR and [O III]/TIR ratios highlight a leaky structure with a large volume filling factor of low density gas and UV photons escaping from dense H II regions and traveling far from the H II regions. However different ISM structure/filling factors may be responsible for the large spread in the [C II]/TIR values. When compared to the Brauher et al. (2008) sample, it is surprising how the dwarf galaxies sometimes occupy a completely different parameter space than the more metal-rich galaxies. The line ratios can be interpreted in terms of excitation of the different FIR lines. In particular, the very high [O III]/[N II] 122 found for the dwarf galaxies is a clear indication of prominent high excitation regions. The low [N II] 122/[C II], relatively low [O I] 63/[C II], and high [O III]/[C II] ratios could be used to investigate [C II] excitation, as the [C II] line can arise in the diffuse ionized, diffuse neutral, or dense neutral phases.

This results in a vivid picture for the ISM of dwarf galaxies, of clumpy PDRs located in a diffuse ionized/neutral medium. Resolving local structures, as is possible in the most nearby objects like the Magellanic Clouds or a few Local Group galaxies (e.g. IC 10), are important next steps to confirm this picture.

5.3 H II region / PDR modeling

In order to understand the properties of the galaxies that give rise to the observed line intensities and ratios, theoretical modeling steps are required. Physical conditions in the dwarf galaxies such as gas densities, temperatures, extinction, radiation field, can be derived from radiative transfer models.

5.3.1 Method

We use the radiative transfer code Cloudy (Ferland et al. 2013), in combination with the spectral synthesis code STARBURST99 (Leitherer et al. 1999), to model the ionized, atomic, and molecular phases. The model consists of a central source of energy, a starburst with properties taken from literature optical studies, located at the center of a spherical cloud. The starburst ionizes the inner edge of the cloud, where the H II region begins, and the radiative transfer is computed step by step progressively into the cloud. A main advantage of using Cloudy compared to other PDR codes is that, depending on where the calculation is stopped, the ionized, atomic, and molecular phases can be treated within one Cloudy model. The ionized gas that is closest to the central source with respect to the other phases that we model separately will yield the best constraints on the properties of the stellar cluster that is powering the model. Therefore, we first derive the best fit model concentrating on the dense H II region diagnostics, which are the *Spitzer* IRS and *Herschel* PACS ionic lines. Following this step, we will assess what this model predicts for the PDR phase. We also opt to assume pressure equilibrium throughout the models. This is particularly important for the density profile between different phases.

5.3.2 Case study: Haro 11

We have first applied our methodology to the brightest galaxy of the DGS: Haro 11 (Cormier et al. 2012). Haro 11 is an IR luminous unresolved starburst galaxy with metallicity $\sim 0.3\,Z_\odot$, composed of 3 main star-forming knots containing ~ 60 super star clusters and hundreds of young clusters (< 3 Myr; e.g. Adamo et al. 2010). While it is extremely bright in the MIR and FIR lines, it has only been detected recently in H I (Machattie et al. 2014) and in CO(1–0) (Cormier et al. 2014).

We have modeled a comprehensive dataset of 20 MIR-FIR fine-structure lines and find that we need three main phases to adequately describe the ISM of Haro 11:

– a compact H II region of density $10^3\,\mathrm{cm}^{-3}$, illuminated by a young starburst of age 3.7 Myr which reproduces the observed emission of the ionic lines ([Ne III], [S III], [S IV], (O III), etc.);
– an adjacent dense PDR of density $10^5\,\mathrm{cm}^{-3}$ and low covering factor ($\sim 10\,\%$) from which the [O I] lines originate;
– an extended diffuse ($n_\mathrm{H} \simeq 10\,\mathrm{cm}^{-3}$) low-ionized/neutral medium that accounts for the [N II], [Ne II], and [C II] emission. In particular, we find that [C II] is mainly associated with the diffuse ionized gas, questioning its use as a PDR tracer in all environments.

Figure 16 shows the geometry of the model (top) and the contribution from each model component to the observed line intensities (bottom). When continued to higher A_V, the PDR model extends to a dense molecular phase which also
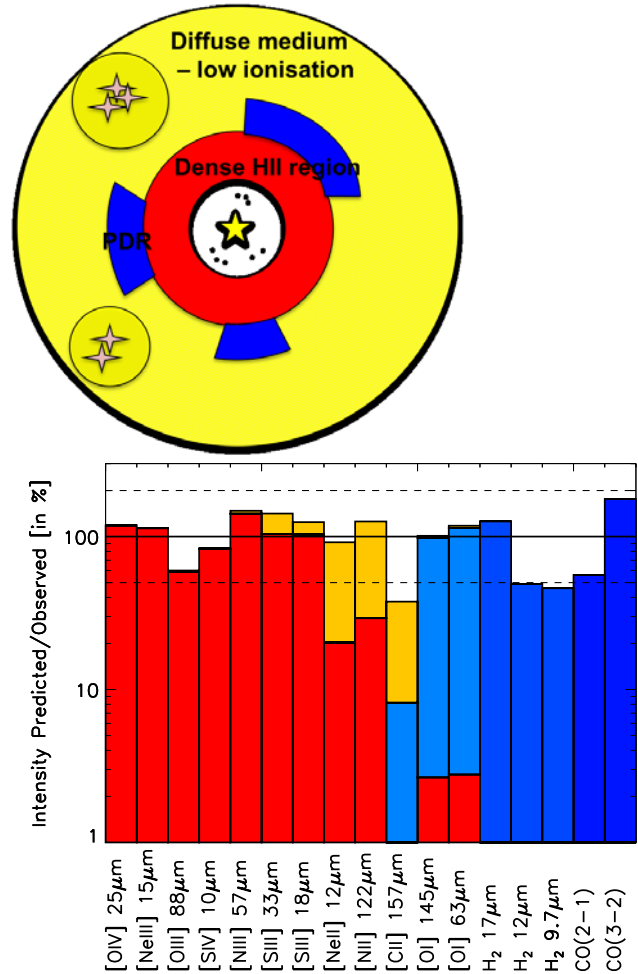

Fig. 16 *Top*: schematic view of the ISM phase composition resulting from our modeling of the IR emission of the starburst dwarf galaxy Haro 11. *Bottom*: intensity contribution of each modeled phase to the observed intensity, for all lines considered. The color coding matches the *top* panel. Adopted from Cormier et al. (2012).

reproduces, within a factor of a few, our recent detections of low-J CO lines.

Our modeling also makes a prediction for the mass residing in each ISM phase, thus yielding a mass budget for Haro 11 where the ionized and atomic gas masses are similar ($\sim 5 \times 10^8\,\mathrm{M}_\odot$) and the molecular mass is the highest $\sim 2 \times 10^9\,\mathrm{M}_\odot$, with about 10 % of if it residing in the CO-dark PDR layer. With such a detailed multi-line study one is thus able to place constraints on the physical conditions in the ISM of Haro 11 and to obtain at least some information on the geometry, even for this unresolved source in which the ISM phases cannot be separated. One of our main results for Haro 11 is that the filling factor of the diffuse ionized gas is much larger than for any other ISM phase. Applying the same methodology to more dwarf galaxies is an important next step to judge whether those results of clumpy PDRs and a large filling factor of diffuse ionized gas are unique to Haro 11 or representative of our sample of star-forming dwarf galaxies.

5.4 Outlook

The ISM of dwarf galaxies is characterized by strong radiation fields which alter their structure and phase distribution, as probed by the *Herschel* lines. In particular, the ionized gas fills a larger volume, and the molecular clouds a smaller volume of the galaxy than in metal-rich galaxies. What is the impact of this structure change on star formation? Despite the low metallicity, the PDR lines of [C II] and [O I] remain efficient coolants of the ISM, but their role in the star formation process is not as evident as for CO as they are usually tracers of the neutral, atomic gas. In order to calibrate them as star formation tracers in galaxies, we need to understand better their phase origin and how their emission depends on physical conditions (e.g. shocks, optical depth effects).

The next step forward to unveil the structure of low metallicity galaxies is to observe their ISM at higher resolution. Radio interferometers (ALMA, NOEMA) will reveal the geometry of the cold ISM, while the airborne SOFIA observatory plays a key role for follow-up FIR studies. With SOFIA (in particular with the FIFI-LS instrument) we will be able to map large areas in nearby galaxies, not only individual star-forming regions, including more quiescent regions of galaxies to probe the FIR emission on small spatial scales *in different environments*. In addition the GREAT instrument with its excellent spectral resolution will allow significant progress to disentangle the possible origins of [C II] in the PDR versus diffuse gas.

References

Abel, N. P., Sarma, A. P., Troland, T. H., & Ferland, G. J. 2007, ApJ, 662, 1024

Adamo, A., Östlin, G., Zackrisson, E., et al. 2010, MNRAS, 407, 870

Begeman K. G., 1987, Ph.D. thesis, Kapteyn Institute, Univ. of Groningen

Bernard-Salas, J., Habart, E., Arab, H., et al. 2012, A&A, 538, A37

Bigiel, F., Leroy, A., Walter, F., et al. 2008, AJ, 136, 2846

Bigiel, F., Leroy, A., Walter, F., et al. 2010a, AJ, 140, 1194

Bigiel, F., Leroy, A., Seibert, M., et al. 2010b, ApJL, 720, L31

Bigiel, F., Leroy, A. K., Walter, F., et al. 2011, ApJ, 730, L13

Bigiel, F., & Blitz, L. 2012, ApJ, 756, 183

Blanc, G. A.,Heiderman, A., Gebhardt, K., et al. 2009, ApJ, 704, 842

Bolatto, A. D., Wolfire, M., & Leroy, A. K. 2013, ARA&A, 51, 207

Blitz, L., & Rosolowsky, E. 2004, ApJ, 612, L29

Bouché, N., Cresci, G., Davies, R., et al. 2007, ApJ, 671, 303

Brauher, J. R., Dale, D. A., & Helou, G. 2008, ApJS, 178, 280

Chonis T. S., Martinez-Delgado D, Gabany R. J., et al. 2011, AJ, 142, 166

Cormier, D., Madden, S. C., Hony, S., et al. 2010, A&A, 518, L57

Cormier, D., Lebouteiller, V., Madden, S. C., et al. 2012, A&A, 548, A20

Cormier, D., Madden, S. C., Lebouteiller, V., et al. 2014, in press, ArXiv:1401.0563

Crosthwaite, L. P., & Turner, J. L. 2007, AJ, 134, 1827

Elmegreen, B. G. 1989, ApJ, 338, 178

Ferland, G. J., Porter, R. L., van Hoof, P. A. M., et al. 2013, Rev. Mexicana Astron. Astrofis., 49, 137

Galliano, F., Madden, S. C., Jones, A. P., et al. 2003, A&A, 407, 159

Gao, Y. & Solomon, P. M. 2004, ApJ, 606, 271

Genzel, R., Tacconi, L. J., Combes, F., et al. 2012, ApJ, 746, 69

Gil de Paz, A., Madore, B. F., Boissier, S., al. 2007, ApJ, 661, 115

Griffin, M. J., Abergel, A., Abreu, A., et al. 2010, A&A, 518, L3

Israel, F. P. & Maloney, P. R. 2011, A&A, 531, A19

Kaufman, M. J., Wolfire, M. G., & Hollenbach, D. J. 2006, ApJ, 644, 283

Kennicutt, R. C., Jr. 1989, ApJ, 344, 685

Kennicutt, R. C., Jr. 1998, ApJ, 498, 541

Kennicutt, R. C., Jr., Calzetti, D., Walter, F., al. 2007, ApJ, 671, 333

Leitherer, C., Schaerer, D., Goldader, J. D., et al. 1999, ApJS, 123, 3

Leroy, A. K., Bolatto, A. D., Simon, J. D., & Blitz, L. 2005, ApJ, 625, 763

Leroy, A. K., Walter, F., Brinks, E., et al. 2008, AJ, 136, 2782

Leroy, A. K., Walter, F., Bigiel, F., et al. 2009, AJ, 137, 4670

Leroy, A. K., Bigiel, F., de Blok, W. J. G., et al. 2012, AJ, 144, 3

Leroy, A. K., Walter, F., Sandstrom, K., et al. 2013, AJ, 146, 19

MacHattie, J. A., Irwin, J. A., Madden, et al. 2014, MNRAS, 438, L66

MacKenty, J. W., Maíz-Apellániz, J., Pickens, et al. 2000, AJ, 120, 3007

Madden, S. C., Poglitsch, A., Geis, N., et al. 1997, ApJ, 483, 200

Madden, S. C. 2000, New A Rev., 44, 249

Madden, S. C., Rémy-Ruyer, A., Galametz, M., et al. 2013, PASP, 125, 600

Marinacci F., Pakmor R., & Springel V., 2014, MNRAS, 437, 1750

Martin, C. L., & Kennicutt, R. C., Jr. 2001, ApJ, 555, 301

Murgia, M., Crapsi, A., Moscadelli, L., & Gregorini, L. 2002, A&A, 385, 412

Poglitsch, A., Krabbe, A., Madden, S. C., et al. 1995, ApJ, 454, 293

Poglitsch, A., Waelkens, C., Geis, N., et al. 2010, A&A, 518, L2

Rahman, N., Bolatto, A. D., Wong, T., al. 2011, ApJ, 730, 72

Regan, M. W., Thornley, M. D., Helfer, T. T., et al. 2001, ApJ, 561, 218

Rubin, D., Hony, S., Madden, S. C., et al. 2009, A&A, 494, 647

Sancisi, R., Fraternali, F., Oosterloo, T., & van der Hulst, T. 2008, A&AR, 15, 189

Schoenmakers R. H. M., Franx M., & de Zeeuw P. T., 1997, MNRAS, 292, 349

Schmidt, M. 1959, ApJ, 129, 243

Schruba, A., Leroy, A. K., Walter, F., et al. 2011, AJ, 142, 37

Schuster, K. F., Kramer, C., Hitschfeld, M., et al. 2007, A&A, 461, 143

Serra, P., Oosterloo, T., Morganti, R., et al. 2012, MNRAS, 422, 1835

Stacey, G. J., Geis, N., Genzel, R., et al. 1991, ApJ, 373, 423

Thilker, D. A., Bianchi, L., Boissier, S., et al. 2005, ApJ, 619, 79

Trachternach C., de Blok W. J. G., Walter F., et al. 2008, AJ, 136, 2720

Walter, F., Brinks, E., de Blok, W. J. G., et al. 2008, AJ, 136, 2563

Wolfire, M. G., Hollenbach, D., & McKee, C. F. 2010, ApJ, 716, 1191

Wong, T., & Blitz, L. 2002, ApJ, 569, 157

Young, L. M., Bureau, M., Davis, T. A., et al. 2011, MNRAS, 414, 940